Torque Characteristics of High Torque Density Partitioned PM Consequent Pole Flux Switching Machines With Flux Barriers

Wasiq Ullah, Faisal Khan, *Member, IEEE*, Erwan Sulaiman, *Member, IEEE,* and Muhammad Umair

***Abstract*—Unique double salient structure of Permanent Magnet Flux Switching Machines (PMFSM) with both Concentrated Armature Winding (CAW) and Permanent Magnet (PM) on stator attract researcher's interest for high speed brushless application when high torque density (T_{den}) and power density (P_{den}) are the primal requirements. However, despite of stator leakage flux, high rare-earth PM usage, PMFSM is subjected to slot effects due to presence of both PM and CAW in stator and partial saturation due to double salient structure which generates cogging torque (T_{cog}), torque ripples (T_{rip}) and lower average torque (T_{avg}). To overcome aforesaid demerits, this paper presents Partitioned PM (PPM) Consequent Pole Flux Switching Machine (PPM-CPFSM) with flux barriers to enhance flux modulation, curtail PM usage and diminish stator leakage flux which reduces slotting effects and partial saturation to ultimately reduces T_{cog} and T_{rip}. In comparison with the existing state of the art, proposed PPM-CPFSM reduces 46.53% of the total PM volume and offer T_{avg} higher up to 88.8%, suppress T_{rip} maximum up to 24.8%, diminish T_{cog} up to 22.74% and offer 2.45 times T_{den} and P_{den}. Furthermore, torque characteristics of proposed PPM-CPFSM is investigated utilizing space harmonics injection i.e. inverse cosine, inverse cosine with 3rd harmonics and rotor pole shaping techniques i.e., eccentric circle, chamfering and notching. Detailed electromagnetic performance analysis reveals that harmonics injection suppressed T_{cog} maximum up to 83.5%, T_{rip} up to 40.72% at the cost of 4.71% T_{avg}. Finally, rotor mechanical stress analysis is utilized for rotor withstand capability and 3D-FEA based Coupled Electromagnetic-Thermal Analysis (CETA) for thermal behavior of the developed PPM-CPFSM. CETA reveals that open space along PPM act as cooling duct that improve heat dissipation.**

***Index Terms*— AC Machines, Consequent Pole, Cogging Torque, Finite element analysis, Permanent Magnet Machine, Torque ripples, Magnetic flux leakages, Harmonics Injection**

I. INTRODUCTION

PERMANENT Magnet (PM) Flux Switching Machines (PMFSMs) are double salient structure, encompassing both Concentrated Armature Winding (CAW) and Permanent Magnet (PM) in stator. PMFSMs housed alternate polarities circumferentially magnetized PM between CAW to fuse with the bipolar changing of CAW flux linkage that result higher magnetic flux density and torque density. Moreover, due to double salient nature the back electromagnetic force (EMF) resemble to sine wave which make it potential candidates for brushless high-speed direct drive application [1] in alternating current mode [2] with significant features i.e., high efficiency, better cooling methods, more efficient, better flux weakening capabilities, torque and power densities [3, 4]. However, despite of high rare-earth PM usage, existing PMFSMs topologies suffer from significant stator leakage flux, cogging torque and torque ripples. Cogging torque is due to double salient structure and slot interaction which result pulsation in instantaneous torque that develop undesirable vibration and acoustics noise [5].

Concerning stator leakage flux, author in [6, 7] utilized mechanical adjustor. Mechanical adjustor eliminates stator leakage flux but despite of high PM usage, this technique requires extra accessories which increases overall machine volume, weight and cost. Author in [8] eliminate leakage flux by introducing C-Core Consequent Pole PMFSM (CPPMFSM) with flux bridges and flux barriers as shown in Fig. 1(a). However, the PM volume increased again in this methodology which increase machine cost. Despite of high PM usage, the narrow flux bridge saturates and provide short path to flux which upsurge flux circulation and cancellation that results an increase cogging torque, torque ripples, low torque density and power density and degrade electromagnetic performance. Concerning the PM usage, author in [9,10] reviewed reduce PM topologies PMFSMs, author in [11] introduces different E-Core and C-Core whereas comprehensive comparison is investigated in [12, 13]. However, reduce PM topologies with C-Core and E-Core still suffer from stator leakage flux (as shown in Fig. 1(b,c,d) and offer low overload capability. The PM usage of conventional and proposed designs are listed in Table I. Author in [14] investigate different topologies of consequent pole and hybrid PMs. However, despite of high PM usage, this design suffers from mechanical constraints. Author [15] studied dual modulation and eliminates flux circulation but in this design the PM volume is doubled. Moreover, since half of the PMs are inserted in rotor pole, these PMs suffers from centrifugal force and de-magnetization. In additional, such designs are not feasible for high speed applications due to mechanical constraints.

Manuscript was submitted for review on 06, December, 2019.
This work receives no funding source yet.
Wasiq Ullah, Faisal Khan and Muhammad Umair are with the Department of Electrical and Computer Engineering, COMSATS University Islamabad, Abbottabad Campus, 22060, Pakistan.
Erwan Suliman is with Department of Electrical Power Engineering, Universiti Tun Hussein Onn Malaysia, 86400 Parit Raja, Johor, Malaysia
(e-mails: wasiqullah014@gmail.com, faisalkhan@cuiatd.edu.pk, muhammadumair1221@gmail.com, erwan@uthm.edu.my)
Digital Object Identifier 10.30941/CESTEMS.2020.00018

TABLE I
PM UTILIZATION IN DESIGN OF PMFSM AND PPM-CPFSM

Design Configuration	PM Usage (mm^3)
12S-10P E-Core PMFSM	10505.75
6S-10P E-Core PMFSM	10505.75
6S-10P C-Core PMFSM	10505.75
12S-14P C-Core CPPMFSM	11856.55
12S-13P E-Core PPM-CPFSM (Proposed Model)	8091.25
6S-13P E-Core PPM-CPFSM (Proposed Model)	8091.25

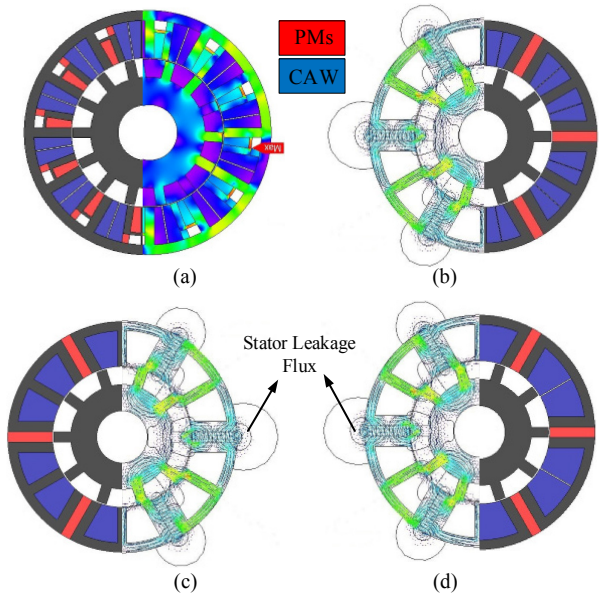

Fig. 1. 2-D Cross sectional view of (a) 12S-14P C-Core CPPMFSM [8] (b) 12S-10P E-Core PMFSM [11] (c) 6S-10P E-Core PMFSM [11] (d) 6S-10P C-Core PMFSM [10]

To compensate foregoing issues of PM usage, stator leakages flux, machine weight, PM cost, flux circulation and cancellation associated with PMFSM and CPFSM, this paper proposes a new Partitioned PM (PPM) Consequent Pole Flux Switching Machine (PPM-CPFSM) with Circumferential Magnetized PMs (CM-PMs) and Radial Magnetized PMs (RM-PMs) as shown in Fig. 2. 2-D cross sectional view with Nephogram shows that proposed new topology of PPM-CPFSM effectively reduced aforesaid PM usage by introducing alternate stator pole to each PM and curtailed the flux circulation and cancellation through flux barriers. In addition, proposed PMCPFSM offer higher average torque, torque density and power density when compare with the conventional existing state of the art.

At this stage, the problem associated with the PM usage and stator leakage flux is successfully curtailed however effects of cogging torque and torque ripples are not accounted. For this purpose, numerous techniques i.e., stator teeth notching [5], pole and slot matching [16, 17], PM shape optimization [18, 19], segmented rotor [20], step skew rotor [21, 22], rotor tooth shapes [2], 3rd harmonics injection in space domain [23, 24] and time domain in control aspect through normal phase current technique [25, 26]. Despite of harmonic injection in space domain, the rest of techniques greatly reduces average torque with cogging torque and torque ripples reduction. Therefore, this paper also implements harmonics injection such as inverse cosine and inverse cosine with 3rd harmonics under different amplitude. Moreover, eccentric circle shaping, notching and chamfering are also investigated for comparison.

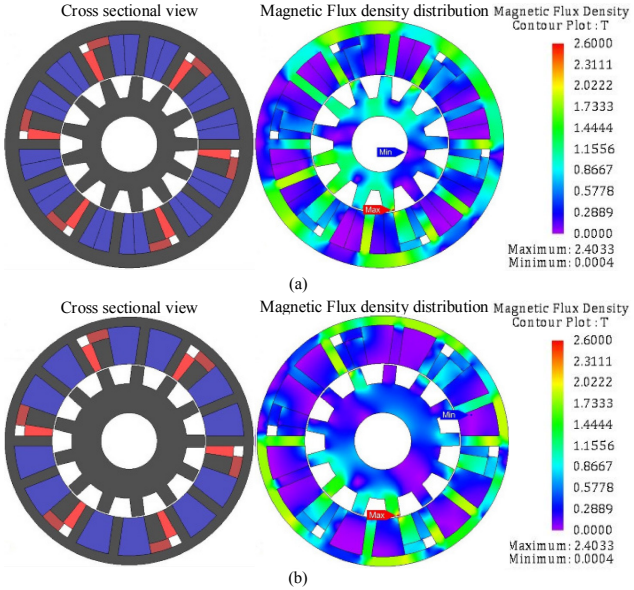

Fig. 2. 2-D Cross sectional view and magnetic flux density distribution of (a) 12S-13P E-Core PPM-CPFSM (b) 6S-13P E-Core PPM-CPFSM

Main contributions of this paper are development of new PPM-CPFSM which successfully reduces PM usage by 46.53%, eliminate stator leakage flux and achieve 88.8% higher torque density. Moreover, inherent cogging torque and torque ripples are effectively curtailed by 83.5% and 40.72% respectively utilizing inverse cosine and inverse cosine with 3rd order harmonics with least sacrifices of average torque. Furthermore, mathematically derived and validated amplitude of injected 3rd order harmonics. In addition, mechanical stress analysis is carried out on rotor for withstand capability and coupled electromagnetic-thermal analysis is developed on 3D FEA for detailed thermal studies. A comprehensive quantitative performance analysis is listed in the proceeding sections.

The rest of the paper is organized as, Section II illustrate structure of proposed PPM-CPFSM, Section III investigate electromagnetic performance analysis of conventional and proposed design Section IV overview rotor pole shaping of PPM-CPFSM, Section V investigates torque characteristics of PPM-CPFSM, Section VI evaluates rotor mechanical stress analysis, Section VII explains briefly coupled electromagnetic-thermal analysis and finally some conclusion is drawn in section VIII.

II. STRUCTURE OF PROPOSED PPM-CPFSM

Geometric design parameters for design of PMFSM and PPM-CPFSM are indicated in Fig. 3 and listed in table II. From Fig. 2, it can be clearly seen that stator of proposed PPM-CPFSM housed two different magnetized partitioned i.e. CM-PMs and RM-PMs. CM-PMs are positioned near stator slot whereas RM-PMs on the top of flux barriers. Magnetization direction of RM-PMs is set opposite to stator leakage flux to enhance main flux linkage and flux barriers are introduces to improve flux modulation effects.

In comparison with the conventional designs (as shown in Fig. 1), the only difference is in the stator structure. Proposed PPM-CPFSM with flux barrier eliminates stator leakage flux and curtailed flux circulation. Hence improve modulation effect which boost torque production capability.

TABLE II
GEOMETRIC DESIGN PARAMETERS OF PMFSM, CPPMFSM AND PPM-CPFSM

Parameter (mm)	E-CORE PPM-CPFSM		C-CORE CPPMFSM	E/C-CORE PMFSM
	6S-13P	12S-13P	12S-14P	12/6S-10P
W_{pm}	2.5	2.1	4	-
H_{pm}	10.1	11.7	9.5	-
H_{fb}	9.5	9.5	10.5	-
D_{sy}	41.6	40	41.4	
H_{rb}	10.2	6.7	10.2	
D_{ro}	27.4	24.7	27.0	
D_{si}	27.9	25.2	27.5	
W_{rp}	4.6	4	3.6	
H_{rp}	6.6	7.9	6.6	
D_{ro}	27.4	26.9	27.0	
H_s	17.1	19.8	17.5	
W_{sy}	3.4	5	3.6	
D_{rs}			10.2	
D_{so}			45.0	
δ			0.5	

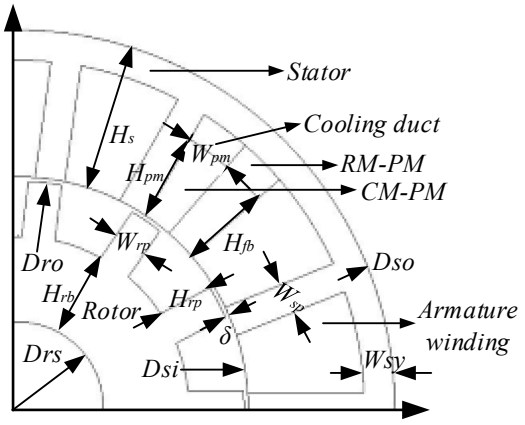

Fig. 3. Definition of design parameters

III. ELECTROMAGNETIC PERFORMANCE ANALYSIS OF CONVENTIONAL AND PROPOSED DESIGN

Electromagnetic performance analysis of conventional design (as shown in Fig. 1) and proposed design (as shown in Fig. 2) with key performance indicators i.e. peak-to-peak cogging torque (T_{cog}), average electromagnetic torque (T_{avg}), torque ripples (T_{rip}), torque density (T_{den}), and power density (P_{den}) are carried out in this section. Aforesaid conventional designs are taken for comparison with proposed design. Extensive electromagnetic performance analysis of proposed PPM-CPFSM is listed in table III whereas for conventional PMFSM and CPPMFSMs are listed in table IV.

In comparison with 12S-10P E-Core PMFSM, the proposed 6S-13P design offers 88.8% higher T_{avg}, reduces T_{rip} by 14.7%, suppress T_{cog} by 22.74% with 2.45 times T_{den} and P_{den} whereas proposed 12S-13P improve T_{avg} by 55.1%, curtailed T_{rip} by 9.91%, reduces T_{cog} by 42.9% with 2.01 times T_{den} and P_{den}.

TABLE III
ELECTROMAGNETIC PERFORMANCE OF PROPOSED PPM-CPFSM

Performance indicator	E-Core PPM-CPFSM Topologies	
	6S-13P	12S-13P
T_{avg} (Nm)	4.25	3.49
T_{cog} (Nm)	2.48	1.83
T_{rip} (Nm)	3.3	2.91
T_{den} $(kNm/m3)$	525.71	431.83
P_{den} (kW/kg)	69.63	57.19

TABLE IV
ELECTROMAGNETIC PERFORMANCE OF CONVENTIONAL PMFSM AND CPPMFSM

Performance indicator	E-Core PMFSM		C-CORE PMFSM	C-CORE CPPMFSM
	12S-10P	6S-10P	6S-10P	12S-14P
T_{avg} (Nm)	2.25	3.83	3.2	3.80
T_{cog} (Nm)	3.21	3.25	2.66	3.22
T_{rip} (Nm)	3.87	3.23	2.54	3.65
T_{den} (kNm/m^3)	214.35	364.93	304.96	321.33
P_{den} (kW/kg)	28.39	48.33	40.39	42.56

Performance analysis with 6S-10P E-Core PMFSM illustrate that proposed 6S-13P design improves T_{avg} by 10.96%, decreases T_{cog} by 23.69%, with 1.44 times T_{den} and P_{den} at the cost of 2.16% increase in T_{rip} whereas proposed 12S-13P reduces T_{avg} by 8.87%, lessen T_{rip} by 24.8%, reduces T_{cog} by 43.69% with 1.18 times T_{den} and P_{den}.

Electromagnetic performance investigation with 6S-10P C-Core PMFSM reveals that proposed design increased T_{avg} by 32.81%, decrease T_{cog} by 6.76% with 1.72 times T_{den} and P_{den} at the cost of 29.9% increase in the T_{rip}. Whereas proposed 12S-13P improve T_{avg} by 9.06%, truncate T_{rip} by 14.56%, reduces T_{cog} by 31.2% with 1.41 times T_{den} and P_{den}.

Analysis in comparison with 12S-14P C-Core CPPMFSM unveil that proposed 6S-13P design improves T_{avg} by 11.84%, shrink T_{cog} by 22.96%, diminish T_{rip} by 9.58% with 1.63 times T_{den} and P_{den}. Whereas proposed 12S-13P offer 8.15% lower T_{avg}, curtailed T_{rip} by 14.56%, reduces T_{cog} by 43.16% and with 1.34 times T_{den} and P_{den}.

Detailed investigation of the electromagnetic performance reveals that proposed 6S-13P E-Core PPM-CPFSM offer maximum up to 88.8% higher T_{avg}, truncate T_{rip} up to 24.8%, suppress T_{cog} up to 22.74% and 2.45 times T_{den} and P_{den} when compared with existing forgoing state of the art. The inner reason of improvement in electromagnetic performance of the developed PPM-CPFSM is the design configuration. From Fig. 2 it can be clearly seen that in proposed PPM-CPFSM, PMs are enclosed in h-shaped stator teeth occupied by CM-PMs and RM-PMs which helps to eliminates stator leakages flux going across the stator yoke (as shown in Fig. 1) thus, converting leakage flux to flux linkage. Moreover, flux modulation effects of both PMs are enhanced to superimpose each other by

introducing flux barriers and results higher magnetic flux density which ultimately improve torque production capability and h-shaped stator teeth with flux barriers reduces PM slot effects to suppress cogging torque and torque ripples. In addition, h-shaped stator teeth provide cooling duct (as shown in Fig. 3) for heat flow to avoid PM demagnetization and overheating and ensure reduce temperature distribution as analyzed in thermal study in the proceeding section. It is also worth mentioning that flux modulation not only occur through stator teeth but also with flux barriers which further improve overall flux circulation and, hence improving overall performance.

In order to further rectify cogging torque and instantaneous torque of the proposed PPM-CPFSM, in the proceeding section torque characteristics are further investigated to mitigate T_{rip} and T_{cog} with least possible sacrifice of T_{avg}.

IV. Rotor Pole Shaping of PPM-CPFSM

In order to investigate torque performance, this section elaborate five different rotor tooth shaping i.e. eccentric circle (Method I), inverse cosine shaping (Method II), inverse cosine with 3rd order harmonics (Method III), chamfering (Method IV) and notching (Method V).

A. Eccentric Circular Shaping

This shaping technique is illustrated in Fig. 4. Rotor pole shows that outline is defined by single arc with given radius. Relation between arc radius, rotor outer diameter and offset distance of arc is given by

$$R_{ec} = D_{ro} - D_{ec} \tag{1}$$

Whereas R_{ec} is radius of eccentric circular arc, D_{ro} outer radius of rotor and D_{ec} is the offset distance for eccentric arc.

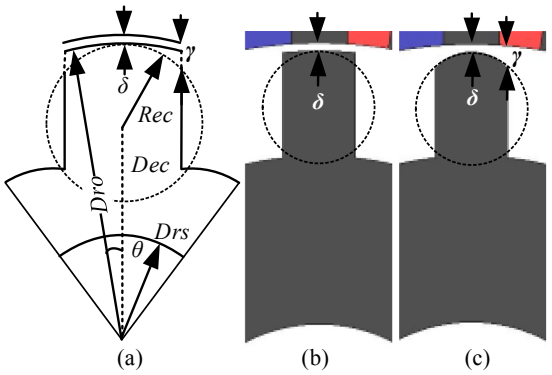

Fig. 4. Schematics of eccentric Circular Shaping (a) Illustration (b) Rotor before Method I (c) Rotor after Method I

In this shaping technique, minimum air gap length (δ) is retained while the air gap length (γ) at the edges of the rotor pole varies with varies with the variation in R_{ec}. While changing $0.88 \leq D_{ec}/D_{ro} \leq 0.96$ the air gap length changes $1.42 \leq \gamma \leq 4.9$ and $0.97 \leq R_{ec} \leq 3.1$. Electromagnetic performance in the preceding structure parameters are illustrated in Fig. 5.

Analysis reveals that utilizing eccentric circle shaping, T_{cog} is reduces from 2.48 Nm to 1.83 Nm and T_{rip} is suppressed

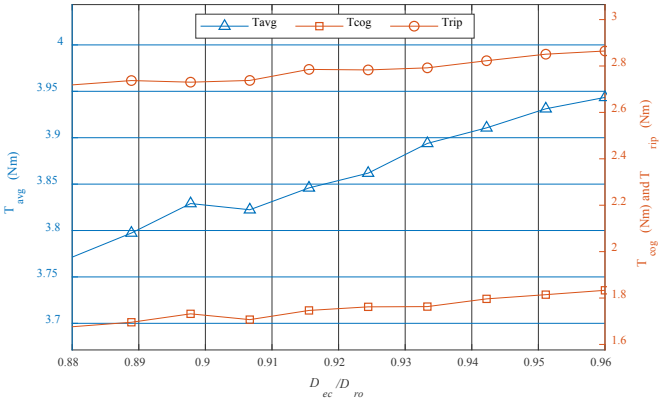

Fig. 5. Influence of eccentric circular shaping on torque characteristics

from 3.34 Nm to 2.86 Nm however, T_{avg} also reduced to 3.94 Nm from 4.25 Nm.

B. Inverse Cosine Shaping

Rotor pole shape have strong influence on air-gap permeance variation. Author in this paper extend this technique to rotor pole shaping for producing air-gap permeance varying in accordance with sin function to result sinusoidal flux distribution to investigate torque behavior. Air-gap permeance vary from $\alpha/2$ (d-axis) toward q-axis as shown in Fig. 6.

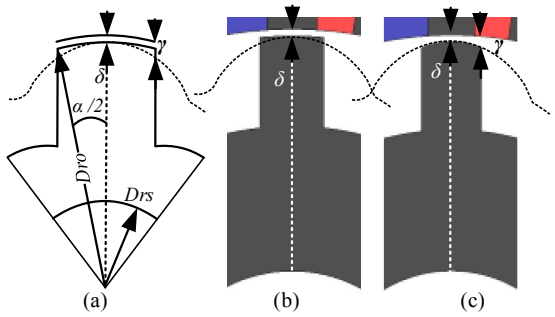

Fig. 6. Schematics of inverse Cosine Shaping (a) Illustration (b) Rotor before Method II (c) Rotor after Method II

During this shaping technique air gap length is altered in accordance of inverse cosine function from d-axis toward q-axis with shaped-arc angle (α), this air-gap length variation can be expressed as [27]

$$\gamma(\alpha) = \frac{\delta}{\cos\left(\frac{\pi}{\tau_p}\alpha\right)}, \quad \alpha \in \left[-\frac{\alpha}{2}, \frac{\alpha}{2}\right] \tag{2}$$

Where τ_p is rotor pole pitch.

Analysis unveil that torque behavior changes with the variation in γ with the change in α. Therefore, γ is vary for different values of α. Variation of torque behavior against γ is shown in Fig. 7.

Analysis reveals that initially when γ is very small, there is slight variation in torque behavior. Moreover, when γ increase T_{avg} abruptly reduces whereas effects of T_{cog} and T_{rip} strengthened rapidly. The only optimum values for γ is found to be 0.85. At optimum γ, T_{cog} is reduces from 2.48 Nm to 0.41 Nm and T_{rip} is suppressed from 3.34 Nm to 1.98 Nm however, T_{avg} slightly reduces to 4.05 Nm from 4.25 Nm.

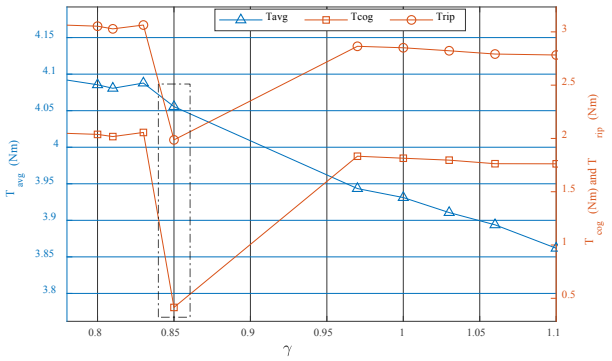

Fig. 7. Investigation of torque characteristics with inverse cosine shaping

C. *Inverse Cosine with 3rd Order Harmonics Shaping*

This is technique is extended from the previous method to enhance torque density in SMPMSM and IPMSM with addition of 3rd order triplen harmonics. Author in this paper, extend this technique to suppress torque ripple and cogging torque while maintaining the average torque. For this purpose, optimal amplitude of 3rd order harmonic is mathematically derived and validate with finite element analysis.

When inverse cosine rotor shape is added with 3rd order harmonics, the air-gap length is modified (as shown in Fig. 8) and express as

$$\gamma(\alpha) = \frac{\delta.k(a)}{\cos\left(\frac{\pi}{\tau_p}\alpha\right) - a.\cos\left(\frac{3\pi}{\tau_p}\alpha\right)}, \quad \alpha \in \left[-\frac{\alpha}{2}, \frac{\alpha}{2}\right] \tag{3}$$

Whereas "a" is amplitude of 3rd order harmonics and k(a) is computed from "a" to have same minimum air-gap length as inverse cosine shape rotor pole.

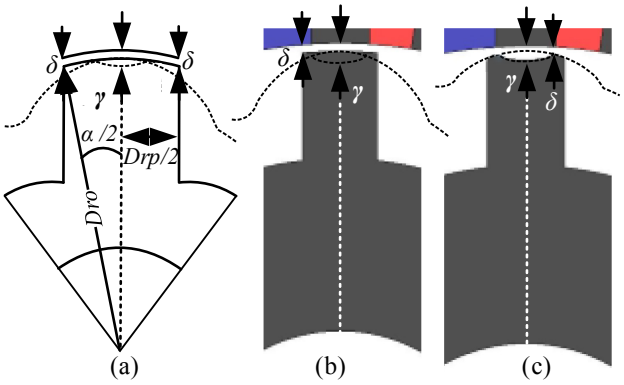

Fig. 8. Schematics of inverse Cosine Shaping with 3rd order harmonics (a) Illustration (b) Rotor before Method III (c) Rotor after Method III

Fig. 8 shows that air-gap length varies along d-axis and q-axis with the addition of different amplitude of 3rd order harmonics. Detail analysis shows that when amplitude of 3rd order harmonics increased, the air-gap length along d-axis increases and q-axis reduces, thus, an optimum amplitude of the 3rd order harmonics need to be calculated and validated to have better torque performance.

In order to search out optimum amplitude of 3rd order harmonics, electromagnetic torque performance $(T_{avg}, T_{cog}, T_{rip})$ is investigated with variation of air-gap length

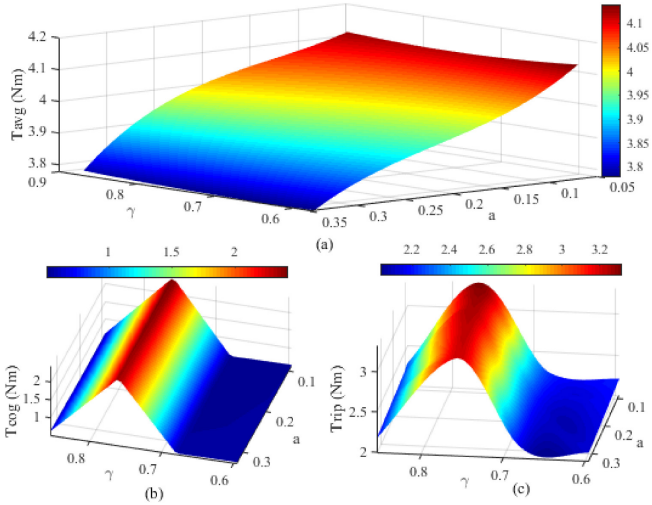

Fig. 9. Effects of 3rd order harmonics on torque characteristics (a) T_{avg} (b) T_{cog} (c) T_{rip}

along q-axis and $a = {}^1/_3, {}^1/_6, {}^1/_9$ and ${}^1/_{12}$ as shown in Fig. 9.

Finite element analysis illustrates that $\gamma = 0.86$ and $a = {}^1/_6$ is optimal point at which T_{cog} is reduced to 0.48 Nm from 2.48 Nm, T_{rip} is suppressed to 2.17 Nm from 3.34 Nm whereas T_{avg} is slightly lower to 4.07 Nm from 4.25 Nm. Moreover, optimum value for "a" is investigated through analytical technique as follow.

In order to modify air-gap permeance and inject 3rd order harmonics with amplitude "a" to sinusoidal flux distribution, the expression to mathematically calculate "a" is modified as

$$y = sin(\theta) + a.sin(3\theta) \tag{4}$$

To find maxima and minima, differentiate "y" with respect to "θ", we have

$$\frac{dy}{d\theta} = \cos(\theta) + 3a.\cos(3\theta) = 0 \tag{5}$$

Whereas

$$3a.\cos(3\theta) = 3a(\cos(2\theta + \theta)) \tag{6}$$

$$3a.\cos(3\theta) = 3a\{\cos(2\theta)\cos(\theta) - \sin(\theta)\sin(2\theta)\} \tag{7}$$

$$3a.\cos(3\theta) = 3a(2\cos^3\theta - \cos\theta - 2\sin^2(\theta)\cos(\theta)) \tag{8}$$

$$3a.\cos(3\theta) = 3a(4\cos^3(\theta) - 3\cos(\theta)) \tag{9}$$

$$3a.\cos(3\theta) = 12a\cos^3(\theta) - 9a\cos(\theta) \tag{10}$$

Replacing (10) in (5),

$$\cos(\theta) + 12a\cos^3(\theta) - 9a\cos(\theta) = 0 \tag{11}$$

$$\cos(\theta)\{1 + 12a\cos^2(\theta) - 9a\} = 0 \tag{12}$$

Either $\cos(\theta) = 0$ or

$$1 + 12a\cos^2(\theta) - 9a = 0 \tag{13}$$

$$\cos(\theta) = \left(\frac{9a-1}{12a}\right)^{1/2} \tag{14}$$

With the addition of 3rd order harmonics, amplitude of "y" is reducing to

$$y = 1 - a \tag{15}$$

$$y = 8a\left(\frac{1+3a}{12a}\right)^{1/2} \tag{16}$$

Now to compute, optimum value of "a", differentiating "y" with respect to "a" and set equal to zero as

$$\frac{dy}{da} = \frac{d}{da}\left(8a\left(\frac{1+3a}{12a}\right)^{\frac{1}{2}}\right) = 0 \quad (17)$$

Solving for "a", we get

$$a = \frac{1}{6} \quad (18)$$

And

$$1 = k(a).0.866 \Rightarrow k(a) = 1.15 \quad (19)$$

Based on finite element analysis and analytical calculation, author conclude that, for rotor pole shaping amplitude of 3rd order harmonics is always $^1/_6$ of the fundamental. Thus, the air-gap length for 3rd order harmonics is modified as

$$\gamma(\alpha) = \frac{1.15.\delta}{\cos\left(\frac{\pi}{\tau_p}\alpha\right) - \frac{1}{6}\cos\left(\frac{3\pi}{\tau_p}\alpha\right)}, \quad \alpha \in \left[-\frac{\alpha}{2}, \frac{\alpha}{2}\right] \quad (20)$$

D. Rotor Pole Chamfering

In this method, the sharp sides edges of the rotor poles are made smooth (as shown in Fig. 10(a)) to provide smooth flux distribution. Since this is previously studied in literature, this technique is implemented here for comparison with the aforesaid techniques. Influence of rotor pole chamfering for various depth (d) of cutting edge is shown in Fig.11. It can be clearly seen that this technique shows very slight influence on torque characteristics of PPM-CPFSM in compare with harmonic injection. Detail analysis shows in this technique T_{cog} is curtailed to 0.50 Nm from 2.48 Nm, T_{rip} is suppressed to 2.21 Nm from 3.34 Nm whereas T_{avg} slightly reduced to 4.23 Nm from 4.25 Nm.

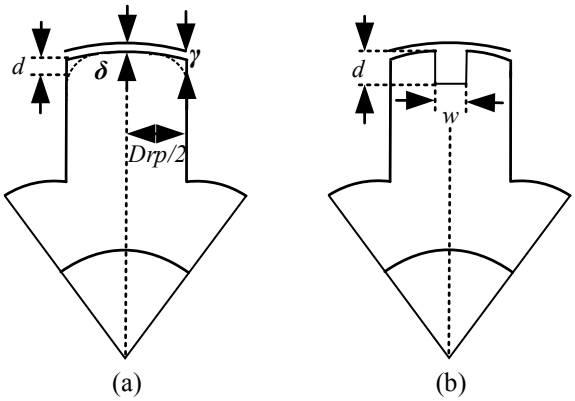

Fig. 10. Schematics of (a) Rotor pole Chamfering (b) Rotor pole Notching

E. Rotor Pole Notching

This technique is also very common for cogging torque reduction in PMFSM. It is implemented here for the sake of comparison. In this section, only one of the notching schemes is studied with varying width (w) and depth (d) as shown in Fig. 10. The electromagnetic performance on torque behavior is shown with varying "w" and "d" is shown in Fig. 12. Analysis illustrate that, T_{rip} is slightly reduced however T_{cog} slightly increased and T_{avg} is reduced. From this, author concluded that rotor tooth notching is effective for cogging torque reduction in PMFSMs but not on PPM-CPFSM.

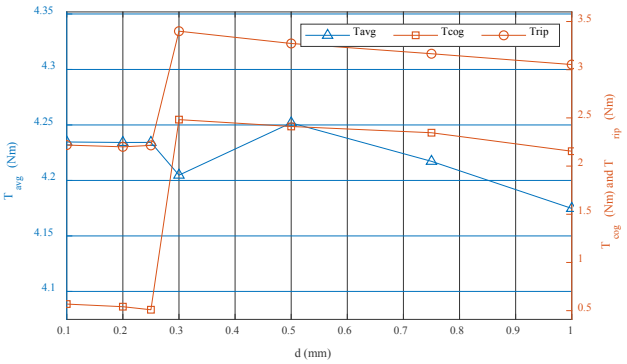

Fig. 11. Effects of rotor pole chamfering on torque performance

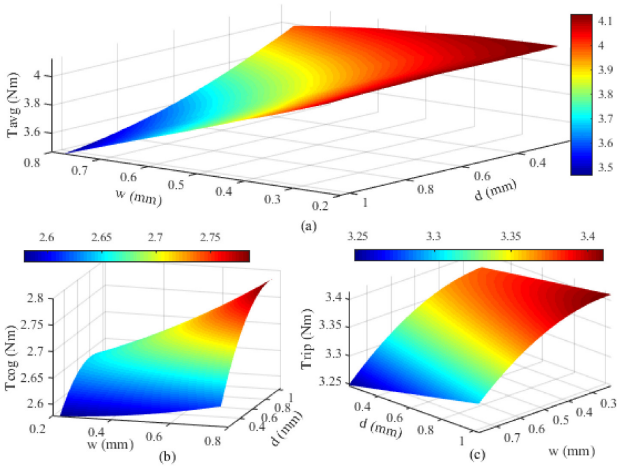

Fig. 12. Investigation of rotor tooth notching on torque characteristics (a) T_{avg} (b) T_{cog} (c) T_{rip}

Detail investigation of the aforesaid rotor pole shaping methods shows great variation in quality of torque profile and electromagnetic performances. The theoretical basis of these variations is mainly due to radial permeance distribution of rotor, flux linkages, magnetic field distribution, average power (P_{avg}), back-EMF, rotor iron losses (R_{IL}), stator iron losses (S_{IL}) and total core losses (T_{CL}) [23, 24].

Electromagnetic performance analysis reveals that during rotor pole shaping magnitude of fundamental component of rotor permeances slightly reduces due to increase in the equivalent air-gap length around the rotor sides causing decrease in the average torque whereas higher order harmonics components are greatly suppressed which truncate related component of T_{rip} and T_{cog}. Moreover, rotor pole shaping unveils that variation in the rotor pole causes variation in the magnitude of the magnetic field distribution and flux linkage as listed in Table V. It is worth mentioning that rotor pole shaping has no influence on flux linkage pattern but only vary air-gap field distribution in the rotor tooth region causing reduction in air-gap permeance which mitigates amplitude of harmonics content and reduces iron loss of rotor and stator as shown in Table V. Analysis leads to the conclusion that despite of torque profile quality, rotor pole shaping helps in reduction of harmonics content, rotor and stator iron losses as well without effecting the pattern of flux linkage.

TABLE V
ELECTROMAGNETIC PERFORMANCE AND IRON LOSSES VARIATION WITH ROTOR POLE SHAPING

Parameter	Original	Method I	Method II	Method III	Method IV	Method V
ϕ_{p-p}(Wb)	0.066	0.060	0.062	0.062	0.066	0.057
ϕ_{THD} (%)	4.22	3.70	3.63	3.16	4.01	2.64
B_{EMF} (V)	106.74	97.61	102.22	102.69	107.26	100.93
P_{avg} (W)	984.53	954.38	960.81	956.15	977.07	934.73
R_{IL}(W)	10.82	10.14	10.42	10.63	10.85	10.36
S_{IL} (W)	40.35	40.04	40.19	40.25	40.32	39.87
T_{CL}(W)	51.17	50.18	50.61	50.88	51.17	50.23

V. TORQUE CHARACTERISTICS OF PPM-CPFSM

This section thoroughly investigates influence of rotor pole shaping on torque performance of the developed PPM-CPFSM and compare with the original initial design. Detail torque characteristics of original design and five rotor poles shaping techniques are listed in Table VI.

TABLE VI
2D FEA BASE COMPARISON OF TORQUE CHARACTERISTICS

Torque (Nm)	Original	Method I	Method II	Method III	Method IV	Method V
T_{avg}	4.25	3.94	4.05	4.07	4.23	3.75
T_{cog}	2.48	1.83	0.41	0.48	0.5	2.71
T_{rip}	3.34	2.86	1.98	2.17	2.21	3.24

Analysis reveals that Method I reduce T_{cog} and T_{rip} by 26.20% and 15.38% respectively at the cost of 7.29% reduction in T_{avg}. Method II suppress T_{cog} and T_{rip} by 83.46% and 40.71% respectively with 4.7% reduction in T_{avg}. Method III curtailed T_{cog} and T_{rip} by 80.64% and 35.02% respectively at the cost of 4.23% reduction in T_{avg}. Method IV diminish T_{cog} and T_{rip} by 79.83% and 33.83% respectively at the cost of 0.47% sacrifices of T_{avg}. Method V weaken $T_{rip}$by 2.99% at the cost of 11.76% reduction in T_{avg} and 9.27% increase in T_{cog} . Waveform of the cogging torque and instantaneous torque is shown in Fig. 13(a) and Fig. 13(b) respectively.

Moreover, average torque capability and effects of torque ripples are investigated under higher current densities (J_s) as shown in Fig. 14. Analysis reveals that as soon as current density increase, average torque increase retaining overload capability. Also, torque ripples initially increase and under higher current densities it become almost constant.

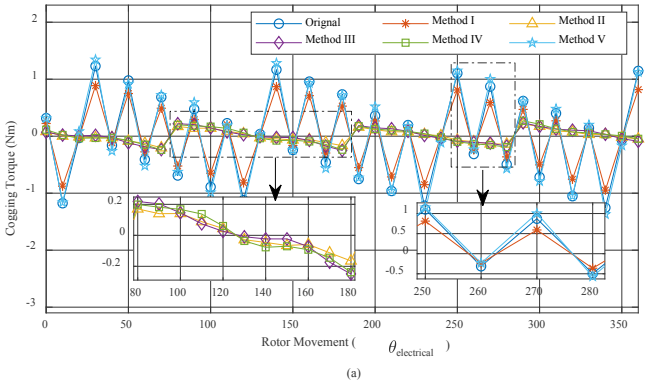

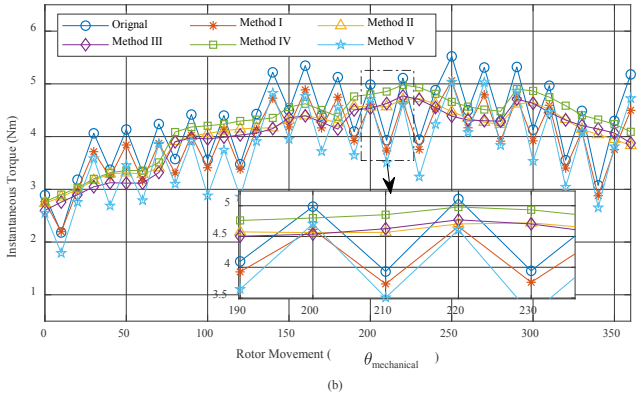

Fig. 13. Comparison of torque waveform (a) cogging torque (b) Instantaneous torque

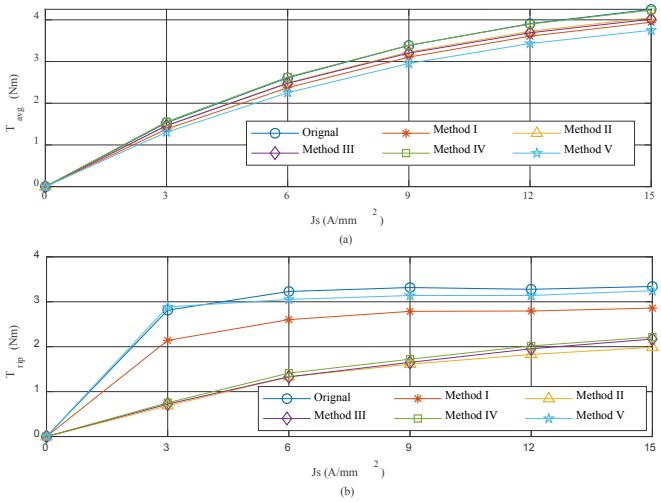

Fig. 14. Influence of J_s on (a) T_{avg} (b) T_{rip}

In this step, influence of applied current and its respective phase are evaluated to choose optimum phase angle of supplied current angle to give higher torque and lowest possible torque ripples. For this purpose, all six designs are tested under various amplitude of applied current and phase angle. Fig. 15(a-f) shows that under different amplitude of applied current maximum torque and minimum torque ripples are achieved when d-axis current is set zero.

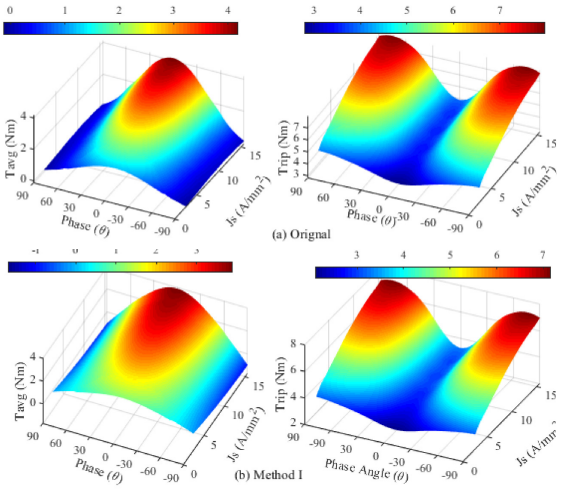

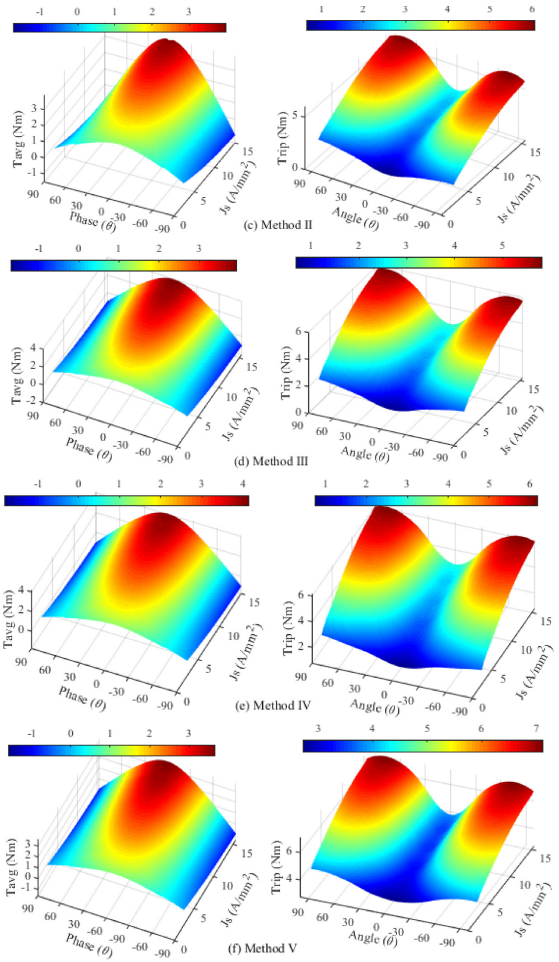

Fig. 15. Influence of J_s and phase angle on T_{avg} and T_{rip} (a) Original (b) Method I (c) Method II (d) Method III (e) Method IV (f) Method V

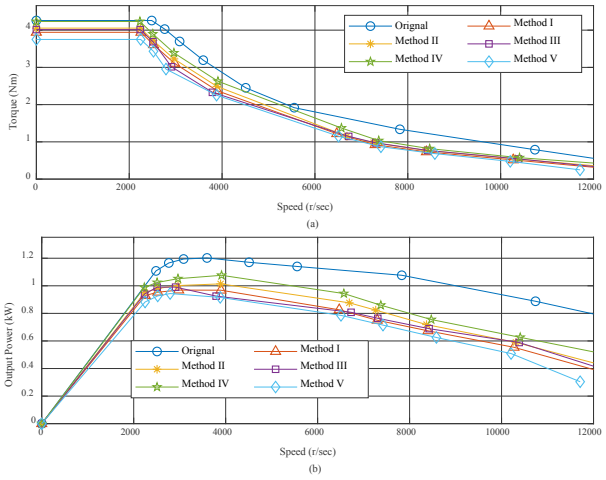

Fig. 16. Characteristics curve of PPM-CPFSM (a) Torque-Speed curve and (b) Power-Speed curve

Finally, all six designs are model and simulated under various current densities for torque and power-speed characteristics as shown in Fig. 16. Detailed analysis unveil that proposed original PPM-CPFSM and modified rotor poles shape are feasible for high speed brushless application.

VI. Rotor Mechanical Stress Analysis

This analysis technique is employed to investigate principal stress occurred in various rotor structures as developed in rotor pole shaping for torque characteristics. Stress analysis on rotor is conducted in such a way that actual condition and constraints are applied in accordance with the material characteristics. Since rotor is subjected to centrifugal rolling force therefore, mechanical stress condition of rotor structure is accomplished by centrifugal force due to longitudinal rotor rotation [28]. This centrifugal force is greatly influenced by angular rotating velocity of rotor therefore analysis is carried out in the wide range of angular velocity to investigate variation of principal stress in various rotor pole shaping methods. In order to examine principal stress on rotor, constraints are set on rotor that coincides to the force acting on rotor pole, rotor tip and rotor back iron (rotor shaft) as shown in Fig. 17.

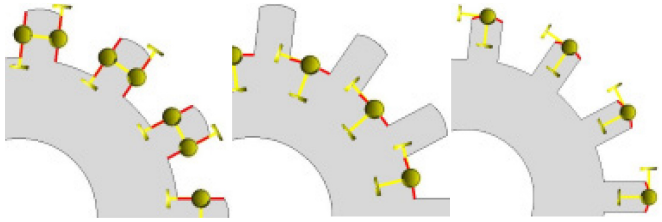

(a) (b) (c)

Fig. 17. Constraints on rotor for stress analysis (a) Rotor pole sides (b) Rotor back iron (c) Rotor Pole tip

Since principal stress on rotor varies with rotating angular speed therefore, analysis is carried out from zero to 30,000 RPMs with difference of 3000 RPM. Fig. 18 shows Nephogram of principal stress on various rotor pole shapes at 30,000 RPM whereas it's variation with speed is illustrated in Fig. 19. This mechanical study of principal stress is carried out on rotor for conventional electromagnetic steel 35H210 having maximum allowable principal stress of 300 MPa.

It is worth mentioning that higher the principal stress for rotor, higher will be the withstand capability [29]. Based on variation of principal stress with rotating speed as shown in Fig. 19 and listed in Table VII, analysis reveals that with the change in rotating speed, principle stress is exponentially increasing. It can be clearly seen that Method IV offer highest withstand capability whereas Method I, Method II and Method III shows intermediate withstand capability but better in comparison with Method V and original rotor structure. Thus, it is concluded that despite of suppressing torque ripples and diminishing cogging torque, rotor pole shaping improves principal stress withstand capabilities, ensure its safe operation under higher speed and make it feasible for high speed applications.

TABLE VII
VARIATION OF PRINCIPAL STRESS WITH ROTATING SPEED

Speed (RPM)	Principal Stress on rotor (MPa)					
	Original	Method I	Method II	Method III	Method IV	Method V
0	0	0	0	0	0	0
3000	0.0585	0.0675	0.0665	0.067	0.1175	0.0592
6000	0.243	0.2701	0.2658	0.2679	0.1175	0.2366
9000	0.5266	0.6077	0.5981	0.6027	1.0578	0.4324
12000	0.9361	1.0803	1.0632	1.0715	1.8875	0.9464
15000	1.4627	1.6879	1.6613	1.6743	2.9383	1.4788
18000	2.1063	2.4306	2.3922	2.4109	4.3212	2.1294
21000	2.8669	3.2083	3.2561	3.2815	5.7592	2.8984

24000	3.7446	4.3211	4.2528	4.2861	7.5222	3.7856
27000	4.7392	5.4689	5.3825	5.4246	9.5202	4.7912
30000	5.8509	6.7517	6.645	6.697	11.7534	5.9151

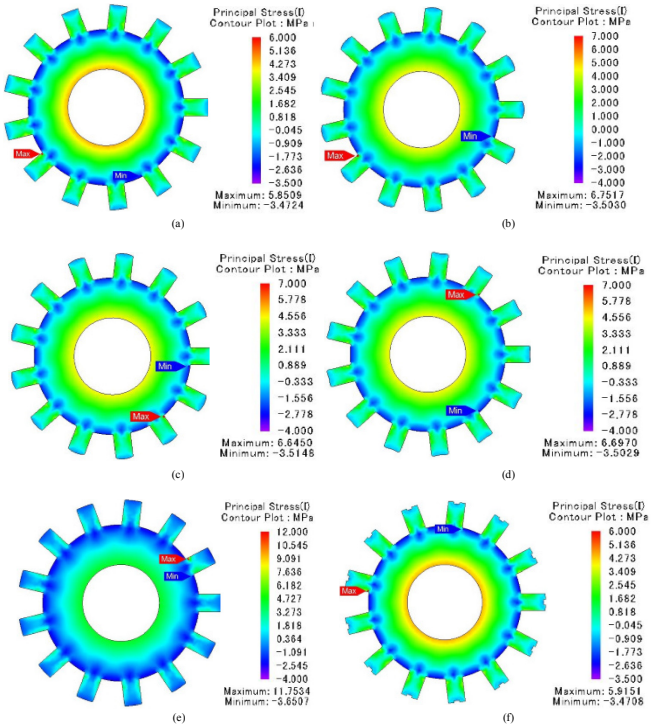

Fig. 18. Nephogram of principal stress at 30,000 RPM in (a) Original (b) Method I (c) Method II (d) Method III (e) Method IV (f) Method V

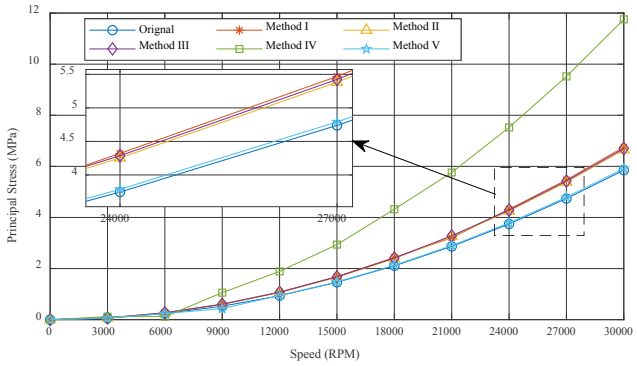

Fig. 19. Variation of principal stress with rotating angular velocity

VII. Coupled Electromagnetic-Thermal Analysis

Temperature rise is critical issue when trying to improve electromagnetic performance of electric machine because the associated machine powers losses act as heat sources [30]. The prominent losses that act as heat source are copper loss, PM Joule loss and iron loss (joule loss and hysteresis loss). Therefore, in order to resolve rise in temperature issues it is important to investigate magnetic study of the design for loss reduction and thermal study for better heat dissipation. Thus, for accurate thermal analysis, it is important to realize amount of heat generated which helps in aforesaid losses calculation in magnetic field transient analysis and extend the result of loss distribution for thermal analysis. In this paper, 3D-FEA based coupled electromagnetic-thermal analysis is carried out to investigate heat generation due to losses distribution and coupled to transient thermal analysis for temperature distribution utilizing JMAG designer V.18.1. The overall workflow of this analysis is shown in Fig. 20.

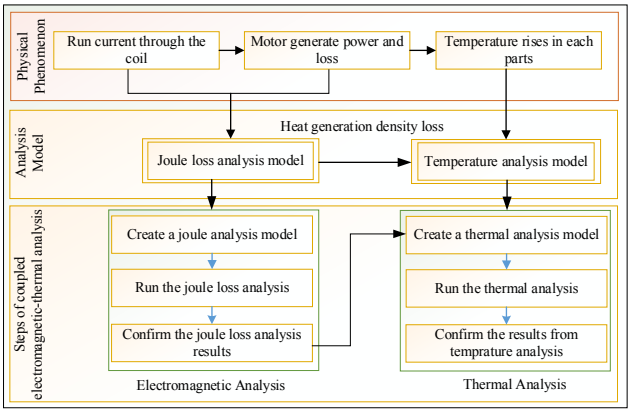

Fig. 20. Physical phenomena and model analysis for coupled electromagnetic-thermal analysis

In this analysis, two different types of models i.e. Joule loss model (Magnetic field analysis) and temperature analysis model (Thermal analysis) are coupled together for investigation during load condition. Initially, current is applied to armature winding that generates power and associated aforesaid losses which results an increase in temperature. Note that copper losses are due to current flow in the armature winding, iron loss are due to variation of magnetic flux and PM Joule losses due to temperature rises. The physical phenomena are divided in to two model analysis. All the losses are modeled as Joule loss model and the associated heat generation causing temperature rise are modeled as temperature analysis model. Temperature distribution in thermal analysis depend upon the amount of heat generation due to loss distribution in transient magnetic field analysis. For this purpose, both the models are carefully studied with the steps of the flow chart.

In thermal analysis model, simplified Heat Equivalent Circuit (HEC) is developed (as shown in Fig. 21) and material properties i.e. thermal conductivity, density and mechanical properties are listed in Table VIII [31, 32]. HEC play major role of heat transfer between machine parts and with the surrounding environment through convection. Moreover, it is utilized for air dissipation formed by rotor rotation. Note that HEC also take consideration of all machine parts which are not modeled in geometry such as shell, rotor shaft, bearings etc.

TABLE VIII
MATERIALS PROPERTIES USED IN THERMAL ANALYSIS

Machine Part	Density (kg/m^3)	Specific heat $(J/kg\ ℃)$	Thermal Conductivity $(W/m\ ℃)$
Stator	7650	460	23
Rotor	7650	460	23
Shell	2680	905	273
Shaft	7800	440	80
Coils	4000	380	380
PMs	7500	450	9
Insulation	1300	1400	0.3
Ambient air	1.26	1000	0.031

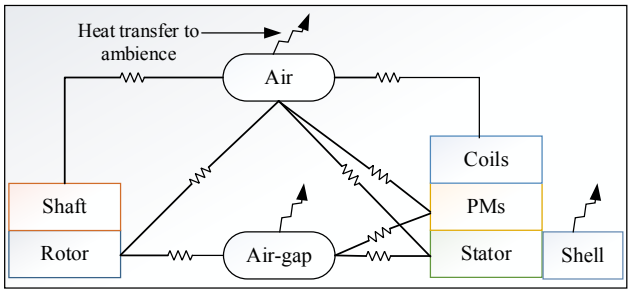

Fig. 21. Heat Equivalent Circuit configuration for proposed PPM-CPFSM

In addition, Heat Transfer Boundary (HTB) are set that link HEC. HTB are used to set the contact faces among different machine parts and air-gap. Finally, Contact Thermal Resistance (CTR) is set between facet component of machine for convection heat transfer. Based on the aforesaid steps and setting, the thermal study is performed and the temperature distribution in proposed PPM-CPFSM is shown in Fig. 22.

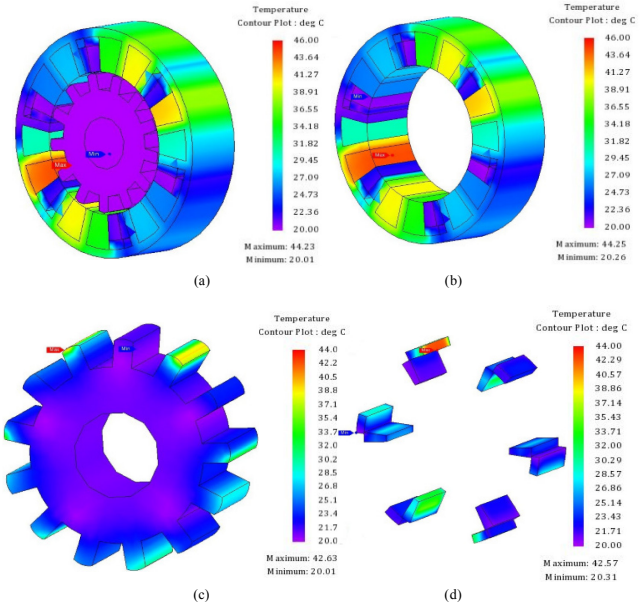

Fig. 22. Temperature distribution in (a) Overall Machine (b) Stator (c) Rotor and (d) Permanent Magnet

3D FEA based temperature distribution under loaded condition shows that overall temperature conditions are very close to each other having maximum at stator coils and minimum at rotor. Analysis reveals that the maximum temperature at stator are 46 ℃ and minimum temperature in the range of 22 ℃ in rotor. Furthermore, the stator temperature is in the range of 41 ℃, 42 ℃ in RM-PMs and 42 ℃ in CM-PMs. Analysis leads to the conclusion that neither PMs nor any machine parts undergoes overheating during loaded condition due to heat dissipation through stator cooling duct between CM-PMs and RM-PMs. Since stator for all designs are same and there is slight variation in rotor teeth causing slight temperature distribution therefore, only one design is analyzed in thermal analysis.

Finally, 3D FEA base transient magnetic study are carried out to make the results more convincing and solid validation of 2D FEA at this stage. 3D cross sectional view with magnetic field distribution are shown in Fig. 23 and corresponding quantitative electromagnetic performance are listed in Table IX. Analysis reveals that 3D FEA bases electromagnetic performance results are inconsistent with 2D FEA results making it more convincing and provide solid validation.

TABLE IX
3D FEA BASE QUANTITATIVE ELECTROMAGNETIC PERFORMANCE

Parameter	Method I	Method II	Method III	Method IV	Method V
T_{avg} (Nm)	3.861	3.942	3.940	4.156	3.679
T_{cog} (Nm)	0.167	0.107	0.155	0.182	0.155
T_{rip} (Nm)	1.930	2.095	2.240	2.360	2.030
ϕ_{p-p} (Wb)	0.0584	0.0615	0.0618	0.0656	0.05751
ϕ_{THD} (%)	3.499	4.012	3.72	4.35	2.8681964
B_{EMF} (V)	95.503	102.52	101.83	106.82	102.064
P_{avg} (W)	917.02	1014.61	1040.26	1052.26	1053.2
R_{IL}(W)	8.895	9.386	9.567	9.912	10.6693
S_{IL} (W)	39.313	37.095	38.94	39.18	

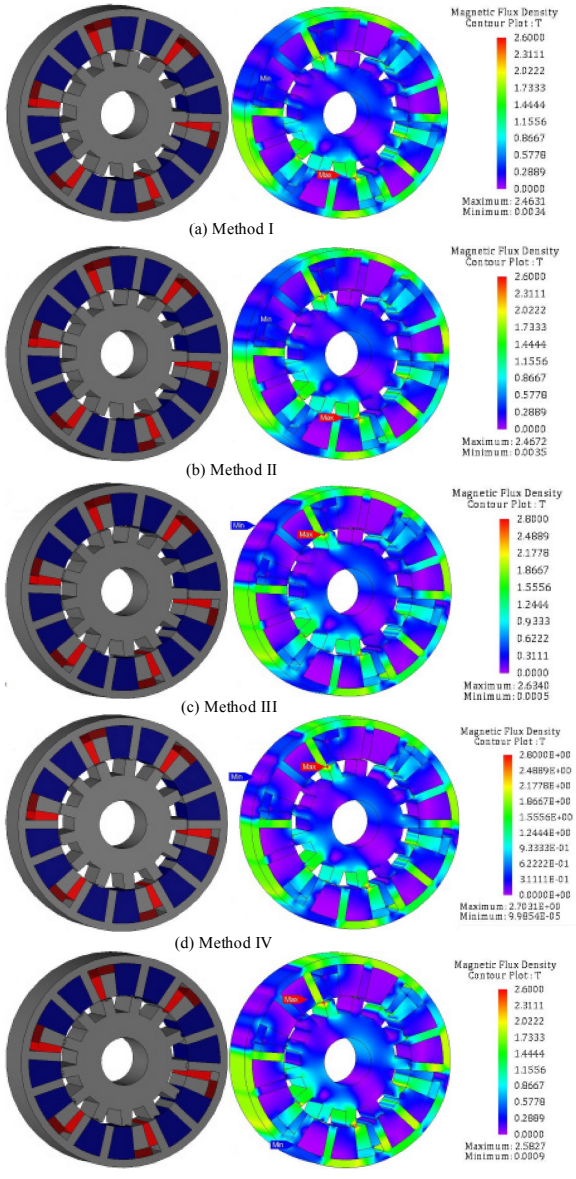

Fig. 23. 3D cross sectional view and magnetic flux density distribution of (a) Method I (b) Method II (c) Method III (d) Method IV (e) Method V

VIII. CONCLUSION

In this paper, a new PPM-CPFSM with flux barriers are investigated which enhance flux modulation and curtail PM usage by 46.53%. Moreover, proposed PPM-CPFSM eliminate stator flux leakage which suppress slotting effects and partial saturation which ultimately reduces T_{cog} and T_{rip} . In comparison with the existing E-Core and C-Core conventional design, the proposed PPM-CPFSM offer T_{avg} higher up to 88.8%, suppress T_{rip} maximum up to 24.8%, diminish T_{cog} up to 22.74% and offer 2.45 times T_{den} and P_{den} at reduce PM usage. Moreover, torque characteristics of proposed PPM-CPFSM is evaluated using space harmonics injection and rotor pole shaping. Detailed electromagnetic performance analysis reveals that harmonics injection suppressed T_{cog} maximum up to 83.5%, T_{rip} up to 40.72% at the cost of 4.71% sacrifice of T_{avg} without effecting overload capability when operating PPM-CPFSM under higher current densities. Moreover, torque-power verse speed characteristics and torque capability are investigated with different current density and phase angle of applied current and achieved that maximum torque and minimum torque ripples at zero d-axis current. Finally, rotor mechanical stress analysis is utilized for rotor withstand capability and 3D-FEA based CETA for thermal behavior of the developed PPM-CPFSM. CETA reveals that open space along PPM act as cooling duct that improve heat dissipation and 3D FEA analysis validate 2D FEA results accurately.

REFERENCES

[1] Z. Q. Zhu, J. T. Chen, Y. Pang, D. Howe, S. Iwasaki and R. Deodhar, "Analysis of a Novel Multi-Tooth Flux-Switching PM Brushless AC Machine for High Torque Direct-Drive Applications," in *IEEE Transactions on Magnetics*, vol. 44, no. 11, pp. 4313-4316, Nov. 2008.

[2] J. Zhao, Y. Yan, B. Li, X. Liu, Z. Chen, "Influence of different rotor teeth shapes on the performance of flux switching permanent magnet machines used for electric vehicles", *Energies*, vol. 12, no. 7, pp. 8056-8075, Dec. 2014.

[3] Noman Ullah, Faisal Khan, Wasiq Ullah, Abdul Basit, Muhammad Umair, Zeeshan Khattak, "Analytical Modelling of Open-Circuit Flux Linkage, Cogging Torque and Electromagnetic Torque for Design of Switched Flux Permanent Magnet Machine," *Journal of Magnetics,* vol. 23, no. 2, pp. 253-266, 2018.

[4] N. Ullah, F. Khan, W. Ullah, M. Umair and Z. Khattak, "Magnetic equivalent circuit models using global reluctance networks methodology for design of permanent magnet flux switching machine," *2018 15th International Bhurban Conference on Applied Sciences and Technology (IBCAST)*, Islamabad, 2018, pp. 397-404.

[5] D. Wang, X. Wang and S. Jung, "Reduction on Cogging Torque in Flux-Switching Permanent Magnet Machine by Teeth Notching Schemes," in *IEEE Transactions on Magnetics*, vol. 48, no. 11, pp. 4228-4231, Nov. 2012.

[6] R. Owen, Z. Q. Zhu, J. B. Wang, D. A. Stone and I. Urquhart, "Mechanically adjusted variable-flux concept for switched flux permanent-magnet machines," *2011 International Conference on Electrical Machines and Systems,* Beijing, 2011, pp. 1-6

[7] Z. Q. Zhu, M. M. J. Al-ani, X. Liu, M. Hasegawa, A. Pride and R. Deodhar, "Comparison of alternate mechanically adjusted variable flux switched flux permanent magnet machines," *2012 IEEE Energy Conversion Congress and Exposition (ECCE),* Raleigh, NC, 2012, pp. 3655-3662.

[8] Y. Gao, D. Li, R. Qu, H. Fang, H. Ding and L. Jing, "Analysis of a Novel Consequent-Pole Flux Switching Permanent Magnet Machine with Flux Bridges in Stator Core," *in IEEE Transactions on Energy Conversion,* vol. 33, no. 4, pp. 2153-2162, Dec. 2018.

[9] Z. Q. Zhu, "Switched flux permanent magnet machines — Innovation continues", *Proc. ICEMS,* pp. 1-10, Aug. 2011.

[10] Z. Q. Zhu and J. T. Chen, "Advanced Flux-Switching Permanent Magnet Brushless Machines," *IEEE Transactions on Magnetics,* vol. 46, no. 6, pp. 1447-1453, June 2010.

[11] J.T. Chen, Z.Q. Zhu, S. Iwasaki et al., "A novel E-core switched-flux PM brushless AC machine", *IEEE Trans. Ind. Appl.*, vol. 47, no. 3, pp. 1273-1282, 2011.

[12] W. Ullah, F. Khan, N. Ullah, M. Umair, B. Khan and H. A. Khan, "Comparative Study Between C-Core/E-Core SFPMM with Consequent Pole SFPMM," *2019 International Symposium on Recent Advances in Electrical Engineering (RAEE)*, Islamabad, Pakistan, 2019, pp. 1-6.

[13] Ullah, Wasiq; Khan, Faisal; Sulaiman, Erwan; Umair, Muhammad; Ullah, Noman; Khan, Bakhtiar: 'Analytical validation of novel consequent pole E-core stator permanent magnet flux switching machine', *IET Electric Power Applications,* 2020, 14, (5), p. 789-796, DOI: 10.1049/iet-epa.2019.0257

[14] J. Li, K. Wang and C. Liu, "Comparative Study of Consequent-Pole and Hybrid-Pole Permanent Magnet Machines," in *IEEE Transactions on Energy Conversion*, vol. 34, no. 2, pp. 701-711, June 2019.

[15] Z. Liang, Y. Gao, D. Li, R. Qu, "Design of a novel dual flux modulation machine with consequent-pole spoke-array permanent magnets in both stator and rotor", *CES Trans. Elect. Mach. Syst.*, vol. 2, no. 1, pp. 73-81, Mar. 2018.

[16] J. T. Chen and Z. Q. Zhu, "Winding Configurations and Optimal Stator and Rotor Pole Combination of Flux-Switching PM Brushless AC Machines," in *IEEE Transactions on Energy Conversion*, vol. 25, no. 2, pp. 293-302, June 2010.

[17] J. T. Chen and Z. Q. Zhu, "Comparison of All- and Alternate-Poles-Wound Flux-Switching PM Machines Having Different Stator and Rotor Pole Numbers," in *IEEE Transactions on Industry Applications*, vol. 46, no. 4, pp. 1406-1415, July-Aug. 2010.

[18] P. Zheng, J. Zhao, J. Han, J. Wang, Z. Yao and R. Liu, "Optimization of the Magnetic Pole Shape of a Permanent-Magnet Synchronous Motor," in *IEEE Transactions on Magnetics*, vol. 43, no. 6, pp. 2531-2533, June 2007.

[19] W. Zhao, T. A. Lipo and B. Kwon, "Material-Efficient Permanent-Magnet Shape for Torque Pulsation Minimization in SPM Motors for Automotive Applications," in *IEEE Transactions on Industrial Electronics*, vol. 61, no. 10, pp. 5779-5787, Oct. 2014.

[20] S. E. Abdollahi and S. Vaez-Zadeh, "Reducing Cogging Torque in Flux Switching Motors With Segmented Rotor," in *IEEE Transactions on Magnetics*, vol. 49, no. 10, pp. 5304-5309, Oct. 2013.

[21] W. Fei, P. C. K. Luk and J. Shen, "Torque Analysis of Permanent-Magnet Flux Switching Machines With Rotor Step Skewing," in *IEEE Transactions on Magnetics*, vol. 48, no. 10, pp. 2664-2673, Oct. 2012.

[22] W. Fei, P. C. K. Luk, J. X. Shen, B. Xia and Y. Wang, "Permanent-Magnet Flux-Switching Integrated Starter Generator With Different Rotor Configurations for Cogging Torque and Torque Ripple Mitigations," in *IEEE Transactions on Industry Applications*, vol. 47, no. 3, pp. 1247-1256, May-June 2011.

[23] L. R. Huang, J. H. Feng, S. Y. Guo, Y. F. Li, J. X. Shi and Z. Q. Zhu, "Rotor Shaping Method for Torque Ripple Mitigation in Variable Flux Reluctance Machines," in *IEEE Transactions on Energy Conversion*, vol. 33, no. 3, pp. 1579-1589, Sept. 2018.

[24] K. Wang, Z. Q. Zhu, "Third Harmonics Utilization in Permanent Magnet Machines", *Springer, Singapore*, September 17, 2018, doi.org/10.1007/978-981-13-0629-7

[25] W. Zhao, M. Cheng, K. T. Chau, R. Cao and J. Ji, "Remedial Injected-Harmonic-Current Operation of Redundant Flux-Switching Permanent-Magnet Motor Drives," in *IEEE Transactions on Industrial Electronics*, vol. 60, no. 1, pp. 151-159, Jan. 2013.

[26] W. Zhao, M. Cheng, R. Cao, and J. Ji, "Experimental comparison of remedial single channel operations for redundant flux-switching permanent-magnet motor drive," Progress In Electromagnetics Research, Vol. 123, 189–204, 2012.

[27] S. A. Evans, "Salient pole shoe shapes of interior permanent magnet synchronous machines," *The XIX International Conference on Electrical Machines - ICEM 2010*, Rome, 2010, pp. 1-6.

[28] J. A. Rani, E. Sulaiman, M. F. Omar, M. Z. Ahmad and F. Khan, "Computational method of rotor stress analysis for various flux switching machine using J-MAG," *2015 IEEE Student Conference on Research and*

Development (SCOReD), Kuala Lumpur, 2015, pp. 721-726.

[29] Ur Rahman, L.; Khan, F.; Khan, M.A.; Ahmad, N.; Khan, H.A.; Shahzad, M.; Ali, S.; Ali, H. Modular Rotor Single Phase Field Excited Flux Switching Machine with Non-Overlapped Windings. *Energies* 2019, *12*, 1576.

[30] L. Mo, X. Zhu, T. Zhang, L. Quan, Y. Wang and J. Huang, "Temperature Rise Calculation of a Flux-Switching Permanent-Magnet Double-Rotor Machine Using Electromagnetic-Thermal Coupling Analysis," in *IEEE Transactions on Magnetics*, vol. 54, no. 3, pp. 1-4, March 2018, Art no. 8201004

[31] G. Zhang, W. Hua, M. Cheng, B. Zhang and X. Guo, "Coupled Magnetic-Thermal Fields Analysis of Water-Cooling Flux-Switching Permanent Magnet Motors by an Axially Segmented Model," in *IEEE Transactions on Magnetics*, vol. 53, no. 6, pp. 1-4, June 2017, Art no. 8106504

[32] Z. Shu, X. Zhu, L. Quan, Y. Du, C. Liu, "Electromagnetic performance evaluation of an outer-rotor flux-switching permanent magnet motor based on electrical-thermal two-way coupling method", *Energies*, vol. 10, no. 5, pp. 677, 2017

Wasiq Ullah is basically from Afghanistan and was born in District Peshawar, Khyber Pakhtunkhwa, Pakistan in 1995. He received his B.S. degrees in electrical (power) engineering from COMSATS University Islamabad (Abbottabad Campus), Abbottabad, Pakistan in 2018. He is currently pursuing M.S. degree in electrical (power) engineering from COMSATS University Islamabad (Abbottabad Campus), Abbottabad, Pakistan.

From 2018 till now, he is Research Associates with Electric Machine Design research group. His research interests include analytical modelling, design analysis and optimization of Permanent Magnet Flux Switching Machines, Linear Flux Switching Machines, Hybrid Excited Flux Switching Machines and novel Consequent pole Flux Switching Machines for high speed brushless AC applications.

Faisal Khan was born in District Charsada, Khyber Pakhtunkhwa, Pakistan in 1986. He received his B.S. degree in electronics engineering from COMSATS University Islamabad (Abbottabad Campus), Pakistan in 2009 and M.S. degree in electrical engineering from COMSATS University Islamabad (Abbottabad Campus), Pakistan in 2012. He received Ph.D. degree in electrical engineering from Universiti Tun Hussein Onn Malaysia, Malaysia in 2017.

From 2010 to 2012, he was a Lecturer at University of Engineering & Technology, Abbottabad, Pakistan. Since 2017, he has been Assistant Professor with the Electrical Engineering Department, COMSATS University Islamabad (Abbottabad Campus), Pakistan. He is author of more than seventy publications, one patent, and received multiple research awards. His research interests include design and analysis of flux-switching machines, synchronous machines, and DC machines.

Erwan Sulaiman was born in Johor, Malaysia, on August 31, 1978. He received his B.E and M.E degrees in Electrical Engineering from University of Malaya in 2001 and University Tun Hussein Onn Malaysia (UTHM) in 2004. He has been with UTHM from December 2004 as a lecturer. He received Doctor Degree in Electrical Engineering from Nagoya Institute of Technology (NIT), Japan in 2012. He is currently professor at Department of Electrical Power Engineering, University Tun Hussein Onn Malaysia. His research interests include design optimizations of Hybrid Excited Flux Switching Machines (HEFSM) and Wound Field Flux Switching Machines (WFFSM) for Electric Vehicles (EVs) and Hybrid Electric Vehicles (HEVs) drive applications.

Muhammad Umair was born in District Peshawar, Khyber Pakhtunkhwa, Pakistan in 1995. He received his B.S. degrees in electrical (power) engineering from COMSATS University Islamabad (Abbottabad Campus), Abbottabad, Pakistan in 2018. He is currently perusing M.S degree in Electrical (Power) Engineering at COMSATS University Islamabad (Abbottabad Campus). His research interests include design, analysis, optimization and experimental validation of flux-switching machines.